Nucleic Acids Research Advance Access published January 19, 2011

Nucleic Acids Research, 2011, 1–12
doi:10.1093/nar/gkq1361

Probing RNA dynamics via longitudinal exchange and CPMG relaxation dispersion NMR spectroscopy using a sensitive ^{13}C-methyl label

Karin Kloiber[1,2], Romana Spitzer[1], Martin Tollinger[1], Robert Konrat[2] and Christoph Kreutz[1,*]

[1]Institute of Organic Chemistry, Leopold Franzens University, Innrain 52a, 6020 Innsbruck and [2]Institute of Computational and Structural Biology, University of Vienna, Max F. Perutz Laboratories, Campus Vienna Biocenter 5, 1030 Vienna, Austria

Received October 8, 2010; Revised December 23, 2010; Accepted December 30, 2010

ABSTRACT

The refolding kinetics of bistable RNA sequences were studied in unperturbed equilibrium via ^{13}C exchange NMR spectroscopy. For this purpose a straightforward labeling technique was elaborated using a 2′-^{13}C-methoxy uridine modification, which was prepared by a two-step synthesis and introduced into RNA using standard protocols. Using ^{13}C longitudinal exchange NMR spectroscopy the refolding kinetics of a 20 nt bistable RNA were characterized at temperatures between 298 and 310 K, yielding the enthalpy and entropy differences between the conformers at equilibrium and the activation energy of the refolding process. The kinetics of a more stable 32 nt bistable RNA could be analyzed by the same approach at elevated temperatures, i.e. at 314 and 316 K. Finally, the dynamics of a multi-stable RNA able to fold into two hairpin- and a pseudo-knotted conformation was studied by ^{13}C relaxation dispersion NMR spectroscopy.

INTRODUCTION

It is only recently that RNA biology has gained a lot of attention, due to the discovery that RNA fulfills a variety of functions apart from its important role in protein synthesis. For instance, so called non-coding RNAs were found to play a vital role in gene regulatory processes, which is impressively documented by the discovery of riboswitch sequences in the 5′- and 3′-untranslated regions of mRNA partitions. These RNAs, comprising an aptamer and expression platform, respond to cellular concentration levels of metabolites by altering their conformations, leading to either up- or down-regulation of a certain gene. Closely related to this new species are RNA based thermometers that switch between distinct folded states depending on temperature, which subsequently yields specific gene expression patterns in response to temperature changes (1–6).

These non-coding ribonucleic acids illustrate a common theme concerning their regulatory function: the existence of distinct folded states of RNA that fulfill different tasks (7–10). Frequently, RNA conformational landscapes comprise several stable structures with only marginal free energy differences. It follows that such RNA sequences can exist in multiple conformations at the same time. Interconversions between different secondary structures represent a common regulatory mechanism for the modulation of RNA function and constitute the basic steps of large-scale conformational transitions. Therefore, the thermodynamics and dynamics of such processes deserve a detailed investigation.

For the purpose of characterizing RNA refolding processes, Höbartner and Micura (8) introduced so-called bistable RNAs, i.e. short sequences which populate two or more conformational substates. These small systems permit a detailed investigation of the dynamic properties of isolated secondary structure elements. In this study we chose bistable RNAs as appropriate model systems for the introduction and the benchmarking of the presented approach.

NMR spectroscopy has proven to be very well suited for monitoring the exchange between distinct folded states of RNA. The kinetics of various bistable RNAs have been determined by applying an experimentally demanding real-time NMR approach that relies on trapping a certain conformation by the introduction of a photolabile protection group. Subsequent laser-induced release of the protection group initiates the return to the equilibrium population of the respective bistable RNA, which is

*To whom correspondence should be addressed. Tel: +43 512 507 5208; Fax: +43 512 507 2892; Email: christoph.kreutz@uibk.ac.at

monitored by observing the imino proton region of the ^{1}H NMR spectrum. The refolding kinetics was found to be remarkably slow with apparent exchange rates (k_{ex}) as low as 0.01 s^{-1} (11–14).

Wenter *et al.* (15) also applied ^{1}H-detected ^{15}N exchange NMR spectroscopy to characterize refolding kinetics of a 34 nt RNA. This sequence had been designed to undergo exchange on a time scale accessible to characterization by longitudinal exchange spectroscopy (<5 s). A major drawback of the presented approach is the dependence on the exchangeable imino protons, thus water exchange rates have to be determined and considered in the analysis of the exchange process (15).

Here, we report a straightforward labeling strategy using 2′-*O*-$^{13}CH_3$ modified uridine as a very sensitive reporter group to study various RNA conformations and the refolding kinetics thereof. Using ^{13}C longitudinal exchange NMR spectroscopy we were able to characterize the refolding of the aforementioned bistable RNAs (8,12,13,16,17). Furthermore, the dynamic behavior of an RNA sequence coexisting in three folded states, i.e. two hairpin-folds and a pseudoknot conformation, was investigated by Carr–Purcell–Meiboom–Gill (CPMG) relaxation dispersion NMR spectroscopy (18–21). To date, only a limited number of CPMG dispersion studies on RNA exist, the reason being that the experiments performed in uniformly ^{13}C-enriched RNA suffer from artifacts introduced by scalar couplings between adjacent carbons (21–24). This problem was recently circumvented by Johnson *et al.* (25) introducing a $^{13}C2'$-, $^{13}C4'$-labeling methodology eliminating perturbing $^{1}J_{CC}$-effects. Alternatively, Al-Hashimi and co-workers (26) introduced an off-resonance ^{13}C $R_{1\rho}$ experiment to study nucleic acid dynamics with exchange life times of 10 ms. With the introduction of the 2′-*O*-$^{13}CH_3$ modified uridine moiety we create a magnetically isolated spin system where CPMG type experiments can be performed in a straightforward way (27). In addition, the approach allows the site-specific modification of the RNA of interest.

MATERIALS AND METHODS

Synthesis of the 2′-*O*-$^{13}CH_3$ modified uridine phosphoramidite (3)

General. NMR spectra were acquired on a Varian 500 MHz *Unity Plus* instrument. Chemical Shifts are reported relative to TMS and referenced to residual proton solvent signal: $CDCl_3$ (7.26 ppm) for ^{1}H NMR spectra and $CDCl_3$ (77.0 ppm) for ^{13}C spectra. ^{31}P shifts are reported relative to external phosphoric acid (85%). ^{1}H assignments are based on COSY experiments. ^{13}C shifts are assigned from a gradient selected phase sensitive HSQC experiment. Silica 60F-254 plates were used for thin layer chromatography (TLC). For flash column chromatography (FC) silica gel 60 (230–400 mesh) was used. All reactions were conducted under argon atmosphere. Reagents and solvents were purchased from Sigma-Aldrich and used without further purification. Organic solvents were extensively dried using freshly activated molecular sieves (4 Å).

5′-*O*-(4,4′)-Dimethoxytrityl-2′-*O*-[^{13}C]-methyluridine (2)

A suspension of 5′-*O*-DMT-anhydrouridine **1** (1 g, 1.9 mmol) was suspended in anhydrous dimethylformamide (30 ml). Then, freshly prepared magnesium [^{13}C]-methoxide (6 eq., 977 mg, 11 mmol) was added. The mixture was heated to 100°C for 2 h. After evaporation of the solvent, the residue was suspended in ethylacetate and washed twice with saturated sodium bicarbonate solution. The organic phase was then washed with water, dried over sodium sulfate and finally the solvent was evaporated. After drying under high vacuum compound **2** was used without further purification in the next step. Yield: 987 mg of **2** as white foam (93%). TLC (CH_2Cl_2/CH_3OH, 95/5): $R_f = 0.7$; ^{1}H NMR(500 MHz, $CDCl_3$): δ 2.60 (d, $J = 9$ Hz, 1H, HO-C(3′)); 3.64 (d, $J_{CH} = 145$ Hz, 3H, $H_3{}^{13}C{-}O(2')$); 3.59 (m, 2H, H_2-C(5′)); 3.81 (m, 7H, H-C(2′) and 2 OCH_3); 4.00 (m, 1H, H-C(4′)); 4.51 (m, 1H, H-C(3′)); 5.28 (d, $J = 8.5$ Hz, 1H, H-C(5)); 5.98 (d, $J = 1$ Hz, 1H, H-C(1′)); 6.86 (m, 4H, H-C(ar)); 7.27–7.41 (m, 9H, H-C(ar)); 8.06 (d, $J = 8.5$ Hz, 1H, H-C(6)); 8.50 (s, br, 1H, NH) ppm; ^{13}C NMR (125 MHz, $CDCl_3$): δ 55.1 (OCH_3); 58.6 (2′-O-$^{13}CH_3$); 68.3 (C(3′)); 83.5 (C(4′)); 84.0 (C(2′)); 87.1 (C(1′)); 102.2 (C(5)); 113.8 (C(ar)); 128.4, 128.6, 130.4 (C(ar)); 140.0 (C(6)) ppm.

5′-*O*-(4,4′)-Dimethoxytrityl-2′-*O*-[^{13}C]-methyluridine 3′-(2-cyanoethyl)-N,N-diisopropyl-phosphoramidite (3)

Compound **2** (530 mg, 0.94 mmol) was dissolved in a mixture of anhydrous methylene chloride (6 ml) and *N*-ethyldimethylamine (10 eq., 1020 µl, 9.4 mmol). After 5 min stirring at room temperature, 2-cyanoethyl-*N*,*N*-diisopropyl-chlorophosphoramidite (1.5 eq., 335 mg, 1.4 mmol) was added dropwise. Stirring was continued for 2.5 h at room temperature. Then a few drops of methanol were added and stirring was again continued for 30 min. The reaction mixture was diluted with methylene chloride and then washed with saturated sodium bicarbonate solution. The organic phase was dried over sodium sulfate, evaporated and the residue dried under high vacuum. The crude product was purified by column chromatography (CC) on silica (hexanes/ethylacetate 50/50 to 40/60 plus 1% NEt_3). Yield: 504 mg of **3** (mixture of diastereoisomeres) as white foam (71%). TLC (hexanes/ethylacetate 30/70): $R_f = 0.7$, 0.5; ^{1}H NMR (500 MHz, $CDCl_3$): δ 1.03−1.29 (m, 24H, $((CH_3)_2CH)_2N$); 2.44, 2.66 (2 m, 4 H, CH_2CN); 3.45−3.61 (m, 16 H, $((CH_3)_2CH)_2N$, $POCH_2$, $H_2{-}C(5')$, $H_3{}^{13}C{-}O(2')$); 3.80 (2s, 12H, OCH_3); 3.91 (m, 2H, H-C(2′)); 3.96 (m $POCH_2$); 4.21, 4.63 (2m, 2H, H−C(4′)); 4.52, 4.66 (2m, 2H, H-C(3′)); 5.21, 5.24 (2d, 2H, $J = 8.0$ Hz, H−C(5)); 5.99, 6.01 (d, $J = 1$ Hz, 2H, H−C(1′)); 6.86 (m, 8H, H−C(ar)); 7.25−7.43 (m, 18H, H−C(ar)); 7.99, 8.08 (d, 2H, $J = 8.0$ Hz, H−C(6)) ppm; ^{31}P NMR (121 MHz, $CDCl_3$): δ 151.47, 150.98 ppm; ESI-MS (m/z): $[M+H]^+$ calcd for [$^{13}C_1$]-$C_{40}H_{49}N_4O_9P$, 761.80; found 761.87.

Solid phase synthesis and deprotection of RNA sequences

The ^{13}C labeled uridine phosphoramidite was used in combination with standard 2′-*O*-TOM protected building blocks (GlenResearch, VA, Sterling) to synthesize RNA sequences **4**, **5** and **6** and the corresponding reference sequences. Custom primer supports PS 200 (GE Healthcare) with an average loading of 80 μmol g^{-1} were used. The sequences were synthesized on a Pharmacia Gene Assembler Plus using RNA standard methods. Amidite (0.1 M) and activator (5-benzylthio-1*H*-tetrazole, 0.25 M) solutions were dried over freshly activated molecular sieves overnight.

The removal of protecting groups and the cleavage from solid support was achieved by treatment with aqueous methylamine (40%, 650 μl) and ethanolic methylamine (8 M, 650 μl) at room temperature for 8 h. After evaporation the 2′-*O*-protecting groups were removed by adding 1 M tetrabutylammonium fluoride (TBAF) in THF (1200 μl). After 14 h at 310 K the reaction was quenched by the addition of 1 M triethylammonium acetate (TEAA, pH 7.0, 1200 μl). The volume was reduced to ~1 ml and then applied on a HiPrep 26/10 desalting column (GE Healthcare). The crude RNAs were eluted with water, evaporated to dryness and dissolved in 1 ml water.

Analysis and purification of RNA sequences

The quality of the crude RNAs was checked via anion exchange chromatography on a Dionex DNAPac PA-100 column (4 × 250 mm) using standard eluents and at elevated temperature (80°C) (28). Purification of the RNA sequence of interest was achieved by applying the crude RNA on a semi-preparative Dionex DNAPac PA-100 column (9 × 250 mm) using the standard protocol (28). The fractions containing the desired RNA were pooled and loaded on a C18 SepPak catridge (Waters) to remove HPLC buffer salts. The RNA triethylammonium salt form was then eluted from the C18 column with water/acetonitrile (1/1, v/v) and lyophilized. To obtain the RNA sodium salt form, the RNAs were treated with a sodium chloride solution (250 mM, 2 × 10 ml) and water (3 × 10 ml) in a Vivaspin 20 ultra-centrifugation unit with a molecular weight cutoff of 3000 (Satorius Stedim). The integrity of the RNAs was further checked by mass spectroscopy on a Finnigan LCQ Advantage MAX ion trap instrumentation connected to an Amersham Ettan micro LC (GE Healthcare).

NMR spectroscopy

The NMR samples were prepared by lyophilization of the RNA sodium salt form. The RNAs were dissolved together with 50 mM sodium arsenate buffer, pH 6.5 in H_2O/D_2O 9/1 (sequence **4**, **S4a**, **S4b**, **6a** and **6b**) or pure D_2O (sequences **5** and **6**). The NMR samples were then heated to 353 K and snap-cooled on ice.

NMR data were acquired on a Varian 'Unity Plus' instrument operating at 11.7 T or on Varian 'Inova' spectrometers operating at 11.7 and 18.8 T at the temperatures indicated below.

^1H NMR spectra of H_2O-samples were acquired using a double-pulsed field gradient spin-echo (DPFGSE) pulse sequence (29). Assignments of the imino proton resonances for bistable sequences **4** and **5** were reported elsewhere (12,30). Assignments of imino proton resonances for sequences **6**, **6a** and **6b** were achieved by jump-and-return homonuclear ^1H-NOESY experiments (31). Gradient selected phase sensitive ^1H, ^{13}C-HSQC spectra were recorded using a standard pulse sequence (with optional WATERGATE water suppression for H_2O samples).

Longitudinal exchange experiments are based on pulse sequences previously published for ^{15}N, yielding ^{13}C, ^1H 2D correlation maps with amplitude modulation of correlation- and exchange-peaks determined by longitudinal exchange rate constants and the kinetics of interconversion (16). For a ~1 mM sample of sequence **4**, arrays of spectra were recorded at 18.8 T at 298, 300, 303, 306 and 310 K with mixing periods of 5, 100, 200, 300, 400, 600, 800 and 1000 ms (the last data point with 1000 ms was omitted at 298 K). The size of the data matrices for each spectrum was 819*64 complex data points, the number of scans was 48 and the interscan delay was 1.2 s (1 s at 298 K) to yield a total measuring time of 23 h at each temperature (17 h at 298 K). Arrays of longitudinal exchange experiments for sequence **5** were recorded at 18.8 T for three temperatures (312, 314 and 316 K) and analyzed at 314/316 K. Mixing times were 5, 100, 200, 300, 400, 400, 500, 600, 700, 800, 900 and 1000 ms, respectively. Data matrices were 1024*18 (the spectral width in the carbon dimension was set to 160 Hz), the number of transients was set to 48 and the interscan delay was 2.6 s, yielding a total experimental time of 20.5 h.

^{13}C CPMG relaxation dispersion experiments on RNA sequence **6** were recorded at 11.7 and 18.8 T using the pulse sequence published by Skrynnikov *et al.* (27) at 300 K with CPMG field strengths of 33.3, 33.3, 66.7, 100, 133.3, 166.7, 200, 233.3, 266.7, 266.7, 300, 333.3 400, 466.7, 600, 600, 700 and 800 Hz. The relaxation delay was 60 ms. 1024*18 (1501*17) complex data points were recorded at 18.8 (11.7) T with the spectral widths in the proton and carbon dimensions set to 5000 and 150.9 Hz (3000 and 94 Hz), respectively. The number of transients was set to 100 (18.8 T) and 92 (11.7 T) and the interscan delay was 2.9 s, yielding a total experimental time of 55 h (18.8 T) and 45 h (11.7 T).

Data analysis

Spectral processing and peak integration were performed using NMRPipe and the NMRDraw software package (32). All subsequent steps were performed using in-house written software written in Matlab (The MathWorks, www.mathworks.com).

Longitudinal exchange experiments. A numerical fitting procedure was employed for the analysis of data obtained of sequences **4** and **5** with the minimization parameter being $\chi^2 = \sqrt{\langle (I^{exp} - I^{calc})^2 \rangle}$. Errors in the extracted rate constants were determined by Monte Carlo analysis where peak intensities were randomly

modulated according to noise levels in the 2D correlation maps. Since we approximated peak volumes by summing over 5×5 ($t1 \times t2$) data points we assumed that initial peak intensities are directly related to the populations of the conformers (33). This approach is justified by comparison to a fitting protocol where initial intensities were fit along with the other parameters. We opted to use the simplified procedure with fixed initial intensities in order to avoid numerical instabilities associated with the larger number of fit parameters. In order to qualitatively account for cross-correlated relaxation of the correlation peaks, the numerical fit was extended to a 4×4 matrix comprising an additional 'effective' magnetization mode for each species that interconvert with the original magnetization mode due to an effective cross-correlated relaxation rate (Supplementary Table S3). This approach was sufficient to ensure the decays of the correlation peaks to be fit correctly, with results virtually unaltered with respect to a numerical approach that disregards cross-correlated relaxation.

CPMG relaxation dispersion. To assess the time-scale of the dynamics of multi-stable RNA **6**, we employed general numerical two-state fits as well as approximations for very slow and very fast exchange on the chemical shift time-scale (34,35). Initial conditions were obtained by an extensive grid search. The goodness of fit was assessed as $\chi^2 = \sqrt{\langle (R_2^{\exp} - R_2^{calc})^2/\sigma^2 \rangle}$, where σ is the standard deviation computed from duplicate experiments. In addition, the reduced χ^2 value was computed for each model. The significance of the respective models was tested with respect to fitting a flat line using F statistics. For every model, a Monte Carlo analysis was performed where errors were estimated on the basis of the duplicate experiments. In addition, a restricted three-state fit was performed with populations and chemical shift differences constrained at values obtained from ^{13}C, ^{1}H correlation maps and assuming only indirect interconversion between conformers **6″** and **6‴** (via **6′**) (for details see Supplementary Table S5).

Arrhenius analysis. The temperature dependence of the equilibrium constant and the rate constants for sequence **4** obtained from longitudinal exchange data was analyzed by linear regression of ln (K) versus 1/T and ln (k_{ij}) versus 1/T, respectively. The equilibrium and activation parameters were computed in each Monte Carlo run yielding the corresponding mean values and standard deviations.

RESULTS AND DISCUSSION

Choice of ^{13}C label

One important reason for the choice of this particular spin label is the comparatively slow relaxation of methyl ^{13}C magnetization, which increases the time-window where slow refolding processes are accessible to observation and analysis by longitudinal exchange NMR spectroscopy. This is particularly important for studying the kinetics of interconversions of the RNAs investigated here as their conformers are expected to interconvert rather slowly; for instance, the exchange between two distinct states of a 34 nt hairpin structure has been shown to occur with refolding rates ranging from 0.00003 to 0.013 s^{-1} at 288 and 313 K (11).

We decided to attach the ^{13}C-methyl group to the 2′-hydroxyl group of the uridine ribose. This labeling scheme was chosen for several reasons: (i) the building block is easily accessible by means of chemical synthesis and (ii) it yields high signal-to-noise ratios in NMR spectra due to the aforementioned favorable relaxation properties. Most importantly, (iii) the label represents a minimally invasive perturbation of the RNA sequence under investigation. The 2′-methoxy modification is a constituent of naturally occurring RNAs, for instance of transfer ribonucleic acids, and has little influence on the native conformation of a given RNA. The modification does not interfere with the C3′-endo sugar conformation favored by RNA and has only a small stabilizing effect resulting in a slightly higher melting temperature (~1–2 K per modification) (36). However, we are aware that the major drawback of the 2′-*O*-$^{13}CH_3$-label is the deletion of the 2′-hydroxyl group, which is important, for instance, in the formation of a hydration spine in the minor groove of double helical RNA structures. Furthermore, the OH-group can be part of non-canonical RNA structural elements, e.g. tetraloops (37–39). The problem can be circumvented by a careful choice of the labeling position, as discussed below.

Synthesis of 2′-*O*-$^{13}CH_3$-labeled uridine phosphoramidite building block

The synthesis of the ^{13}C labeled uridine building block started from 5′-*O*-DMT-2′-deoxyanhydrouridine **1**, which was prepared according to published procedures (Scheme 1) (40). Compound **1** was quantitatively converted into the 2′-*O*-$^{13}CH_3$-labeled intermediate **2** by treatment with $Mg(O^{13}CH_3)_2$, which was freshly prepared from magnesium turnings and ^{13}C labeled methanol in analogy to earlier works using unlabeled methanol (41). Subsequent phosphitylation with (2-cyanoethyl)-*N*, *N*-diisopropylchlorophosphoramidite provided the desired 2′-*O*-$^{13}CH_3$-labeled uridine building block **3** with

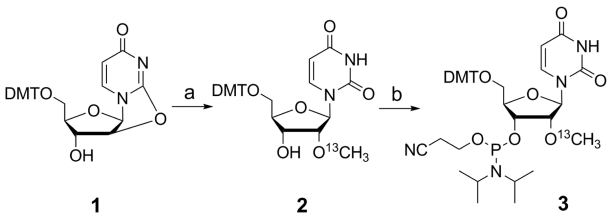

Scheme 1. Synthesis of the 2′-*O*-$^{13}CH_3$-uridine phosphoramidite **3**; (a) 6 eq. ^{13}C-magnesium methoxide [$Mg(O^{13}CH_3)_2$, freshly prepared from magnesium turnings and $^{13}CH_3OH$] in anhydrous dimethylformamide, 100°C, 2 h, 93%; (b) 1.5 eq. (2-cyanoethyl)-*N*,*N*-diisopropylchlorophosphoramidite, 10 eq. *N*-ethyldimethylamine in anhydrous dichloromethane, room temperature, 2.5 h, 71%.

66% overall yield in two steps with one chromatographic purification step. The ^{13}C building block **3** was then used in RNA solid-phase synthesis and was incorporated with >98% coupling efficiency. The molecular weights of the ^{13}C-labeled RNAs were confirmed by LC-ESI mass spectroscopy (Supplementary Table S1).

Labeling strategy, studied RNA sequences and NMR spectroscopic characterization of the individual folds

One of the key steps is the 'correct' choice of the labeling position. The 2′-*O*-$^{13}CH_3$-modified uridine was placed in such a manner that the label is residing in a solvent accessible single stranded position in one of the folds, whereas in the competing conformation the ^{13}C-methyl modified uridine is part of a double helical A-form hairpin stem. Thereby, the magnetic environment is expected to be sufficiently different for the chemical shifts of the competing states to be resolved in an NMR spectrum. The labeling strategy was chosen in line with earlier observations (28).

The realization of the concept was demonstrated by introducing the ^{13}C-uridine **3** into the 20 nt bistable RNA sequence **4** at position 18 (Figure 1A) (12). We observed two distinct signal patterns in both the imino proton regions of the ^{1}H-NMR spectrum and in the ^{1}H, ^{13}C-HSQC spectrum of sequence **4** originating from the two competing folds, **4′** and **4″**, indicating that the two species refold slowly on the NMR chemical shift time-scale (Figure 1B and C). This nicely demonstrates the sensitivity of the isotope label to its magnetic environment. The ^{13}C, ^{1}H resonances were assigned to their respective conformations by the aid of truncated reference sequences (sequences **S4a** and **S4b**, Supplementary Figure S1). Quantification of the equilibrium fold distribution was checked on one hand by the comparative imino proton method [for a detailed description of the comparative imino proton method see reference (8)] and on the other hand by integration of the ^{1}H, ^{13}C-HSQC peaks. Both methods reported the two states to be equally populated, in line with earlier findings (8,12). Importantly, the ^{13}C-modification also proved to be minimally invasive as no population differences compared to the wild-type sequence were found. This was further supported by UV-melting experiments, which show that the 2′-*O*-methoxy modification change the melting transition by only 1–2 K (Supplementary Figure S3) (8).

In order to further explore the applicability of this novel ^{13}C RNA labeling methodology we modified the larger bistable RNA **5** comprising 32 nt with a 2′-*O*-$^{13}CH_3$-uridine building block at position 26 (Figure 1D). For this medium sized RNA sequence **5** severely overlapping signals in the region between 12.5 and 13.5 ppm of the ^{1}H-NMR spectrum were encountered (Figure 1E). So far, only partial assignment of the NH resonances has been achieved by site-specific ^{15}N labeling (30).

This case of resonance overlap demonstrates the potential of our site-specific ^{13}C labeling strategy. Again, two well separated ^{1}H, ^{13}C-HSQC resonances are detected and assigned to the individual folds by comparison with a truncated reference sequence (sequence **S5a**, Supplementary Figure S2). Quantification of the equilibrium population distribution was obtained from 2D peak integration to yield relative populations of folds **5′** and **5″** of ~7/3 (Figure 1F). Of note, the ^{13}C uridine label resides in a single stranded region in both conformations. This leads to a less pronounced chemical shift difference in both dimensions as compared to sequence **4** ($\Delta\omega^{1}H_{4'4''} = 0.305$ ppm, $\Delta\omega^{1}H_{5'5''} = 0.17$ ppm and $\Delta\omega^{13}C_{4'4''} = 1.33$ ppm, $\Delta\omega^{13}C_{5'5''} = 0.31$ ppm). However, the chemical shift differences between the two states in the carbon and proton dimensions are still sufficient to

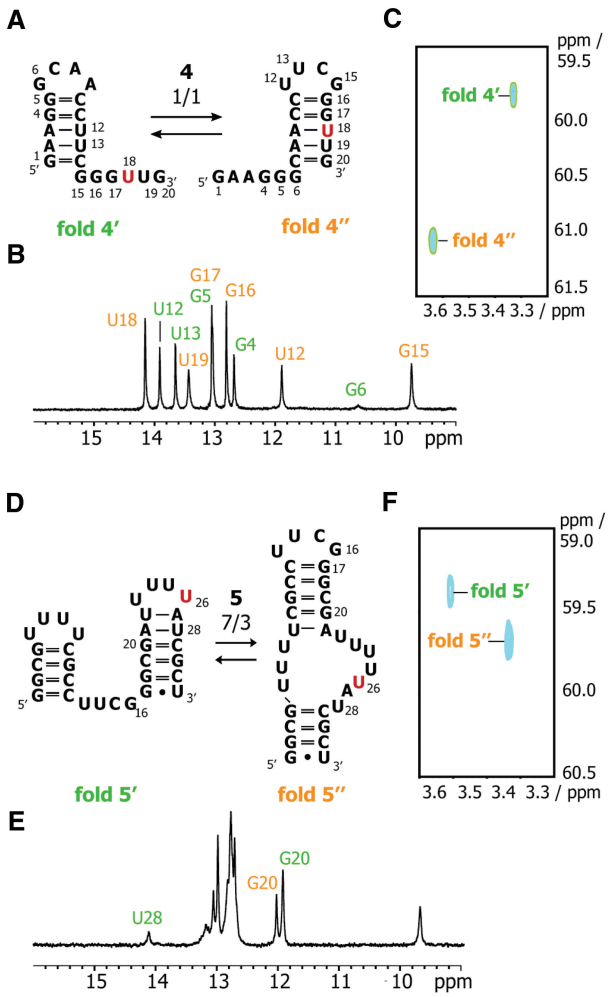

Figure 1. Realization of the presented approach as exemplified on two bistable RNAs (**4** and **5**). (**A**) Bistable 20 nt RNA **4** with the two competing folds **4′** and **4″**. The red U denotes the 2′-*O*-$^{13}CH_3$-uridine label. (**B**) Detection of the folding equilibrium of conformation **4′** and **4″** by analysis of the imino proton region of the ^{1}H NMR spectrum. (**C**) ^{1}H, ^{13}C-HSQC of RNA sequence **4**. The two folding states give rise to two well-resolved peaks in the HSQC spectrum. Assignment was achieved by means of truncated reference sequences (Supplementary Information). (**D**) Bistable 32 nt RNA **5** with the two competing folds **5′** and **5″**. The red U denotes the 2′-*O*-$^{13}CH_3$-uridine label. (**E**) Severe resonance overlap is found in the imino proton region of the ^{1}H NMR spectrum. (**F**) ^{1}H, ^{13}C-HSQC spectrum of RNA sequence **5**. The two conformations are nicely resolved in the HSQC spectrum. Fold assignment was achieved using a truncated reference sequence (**S5a**, see Supplementary Information). Conditions: 0.8–1.0 mM RNA, 50 mM sodium phosphate, pH 6.5, H_2O/D_2O 9/1, 298 K.

distinguish the two states. This observation further strengthens the impact of the presented methodology, as slight deviations from the suggested labeling strategy (single-stranded versus double-stranded) seem to be tolerated. The ratio of peak integrals of folds **5′** and **5″** was 7/3, which is identical to the one given in reference (30), proving that the label did not affect the thermodynamic equilibrium of the conformations. Differences in melting temperatures between wild-type and modified samples determined from UV-melting experiments were very small with ΔT_m (2′-*O*-CH_3 versus wild-type) values between 0.5 and 1 K (T_m^1 (**5**) = 55.8°C, T_m^2 (**5**) = 85.8°C versus T_m^1 (**5WT**) = 55.0°C, T_m^2 (**5WT**) = 85.3°C and T_m (**S5a**) = 70.6°C versus T_m (**S5aWT**) = 69.8°C, Supplementary Figure S3) (8). These findings demonstrate the minimally invasive nature of our modification.

As a final example RNA sequence **6** was chosen (18,19). The oligonucleotide **6** coexists in three competing folds, a pseudoknotted conformation **6′**, a 5′-hairpin fold **6″** and a 3′-hairpin fold **6‴** (Figure 2A). The presence of multiple folding states is not directly observable by the imino proton resonances, as the NH resonances originating from all three conformations (Ψ-knot sequence **6′**, 5′-hairpin **6″** and 3′-hairpin **6‴**) are strongly overlapping (Figure 2B).

The coexistence of the three folding states was revealed by the presence of three observable resonances in the ^{1}H, ^{13}C correlation map of RNA **6** (Figure 2C). By incorporation of the 2′-*O*-^{13}C-methyl uridine label into sequence **6** at position 16 and into the respective reference sequences (**6a** and **6b**), it was possible to assign the methyl ^{1}H/^{13}C resonances. Peak integration of the ^{1}H, ^{13}C-HSQC correlation maps yields an estimate of the individual populations, namely a ratio of ~4/1/2 of pseudoknot **6′**, 5′-hairpin **6″** and 3′-hairpin **6‴** at 298 K. The population distribution was found to be strongly temperature dependent according to peak volumes obtained at various temperatures (278, 283, 298 and 303 K, Figure 3B). While the pseudoknotted conformation **6′** was favored at lower temperatures, the hairpin folds **6″** and **6‴** were increasingly populated at higher temperatures (Figure 3C). This strong temperature dependence is indicative of enthalpy–entropy compensation determining the equilibrium distributions of the three species. Whereas the pseudoknotted conformation is enthalpically favored (8 bp), it is entropically destabilized with respect to the hairpin structures that have long unstructured regions.

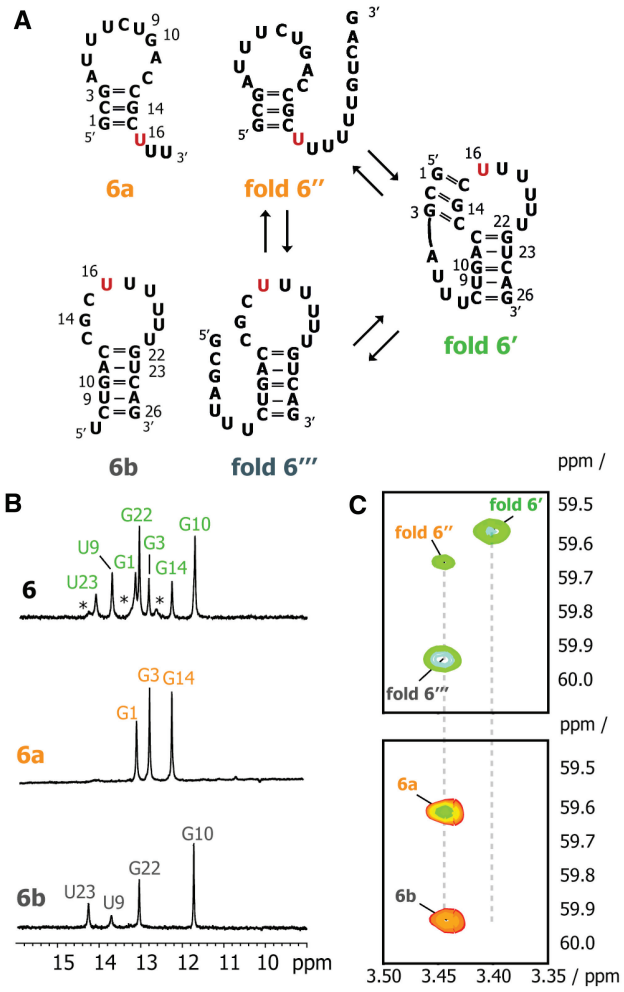

Figure 2. (**A**) Multi-stable RNA sequence **6** is able to fold into a pseudoknotted conformation **6′** and two hairpin structures **6″** and **6‴**. Truncated reference sequences **6a** and **6b** mimic fold **6″** and **6‴**, respectively. The red U denotes the 2′-*O*-$^{13}CH_3$-uridine label. (**B**) Imino proton region of the ^{1}H NMR spectrum of sequence **6** and references **6a** and **6b**. The detection of multiple conformations of RNA **6** is hampered due to NH resonance overlap originating from the individual folds. Asterisks denote unassigned peaks most likely originating from fold **6″** and **6‴**. (**C**) ^{1}H, ^{13}C-HSQC of RNA sequence **6**. The three possible folding states can be easily detected and assigned in the HSQC spectrum. Fold assignment was achieved with truncated reference sequences **6a** and **6b**. Here, an overlay of the HSQC spectra of **6a** and **6b** is shown. Conditions: 0.75 mM RNA, 2.5 mM $MgCl_2$, 50 mM sodium phosphate, pH 6.5, H_2O/D_2O 9/1, 298 K.

Refolding kinetics and conformational dynamics studied by longitudinal-exchange and CPMG NMR experiments

One of our main goals was to determine the refolding kinetics of our model systems at unperturbed equilibrium. RNA sequences **4**, **5** and **6** are expected to interconvert between their conformational substates on time scales ranging from milliseconds to a few seconds. There are several NMR-based methods that are suited to characterize processes occurring at various time scales (42). Motions in the millisecond to microsecond time regime can be characterized using CPMG relaxation dispersion NMR methods (20). Dynamics occurring on the order of a few seconds can be studied by longitudinal exchange experiments, whereas even slower rearrangements can be studied by real-time NMR methods (14,43).

First, we have determined the kinetics of interconversion between the two magnetic environments of the uridine 2′-*O*-$^{13}CH_3$ label in the RNA sequence **4** by ^{13}C longitudinal exchange experiments. This process was previously studied via a fold-caging-real-time NMR approach (12), yielding surprisingly slow refolding kinetics [$k_{ex} = k_{4'\rightarrow4''} + k_{4''\rightarrow4'}$ ranged between 0.01 (at 283 K) and 0.2 s^{-1} (298 K)]. These results were used to benchmark the new labeling scheme and its influence on the kinetic properties of this RNA sequence (12).

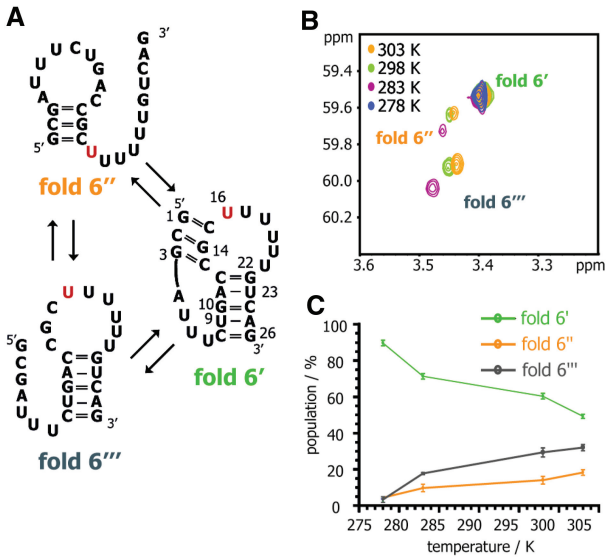

Figure 3. Temperature dependence of folding state populations of RNA sequence **6**. (**A**) Representation of the three possible folding states. The red U denotes the 2′-*O*-$^{13}CH_3$-uridine label. (**B**) ^{1}H, ^{13}C-HSQC spectra of RNA sequence **6** at various temperatures ranging from 278 to 303 K. (**C**) Folding state populations (in %) versus temperature. The populations were determined as the mean value from three independent HSQC measurements at the indicated temperature (error bars from standard deviation). Conditions: 0.75 mM RNA, 2.5 mM $MgCl_2$, 50 mM sodium phosphate, pH 6.5, H_2O/D_2O 9/1, 298 K.

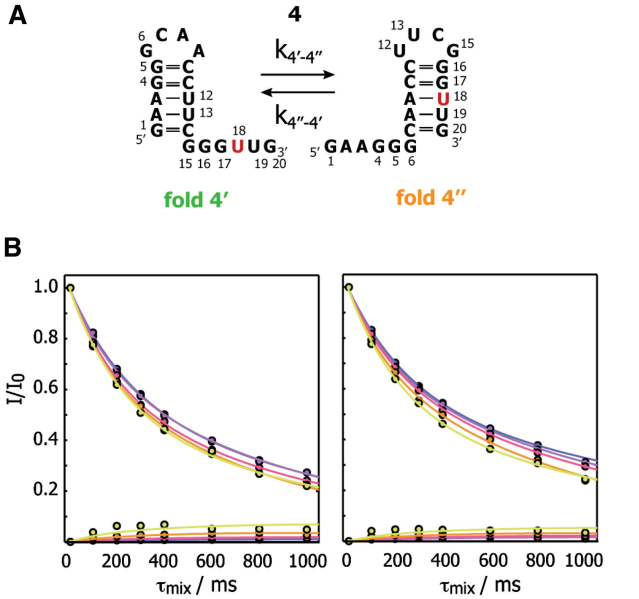

Figure 4. Kinetics of sequence **4** analyzed by ^{13}C longitudinal exchange spectroscopy. (**A**) Interconversion between conformations **4′** and **4″**. The uridine nucleotide that serves as a sensor is highlighted in red. (**B**) Signal intensities as a function of mixing time are shown for a set of temperatures. The left panel shows normalized intensities of the correlation peak of conformation **4′** and the exchange peak corresponding to transition **4′** → **4″**. The right panel depicts the intensities of the correlation peak of conformation **4″** and the exchange peak corresponding to transition **4″** → **4′**. Experiments performed at different temperatures are color-coded (298 K: blue, 300 K: magenta, 303 K: red, 306 K: orange, 310 K: yellow).

We recorded a ^{13}C, ^{1}H resolved longitudinal exchange experiment which yields a series of ^{13}C, ^{1}H correlation maps with correlation- and exchange-peaks that have been amplitude modulated during a mixing time according to their longitudinal relaxation rates and their kinetics of interconversion. Decays and buildups at the different temperatures are shown in Figure 4. Assuming a two-state process we determined the refolding kinetics in the temperature range between 298 and 310 K yielding microscopic exchange rate constants $k_{4'\rightarrow4''}$ between 0.05 and 0.42 s^{-1} and $k_{4''\rightarrow4'}$ between 0.04 and 0.16 s^{-1}, with errors being on the order of 5–10% (Table 1). This corresponds to an exchange rate constant k_{ex} ($k_{ex} = k_{4'\rightarrow4''} + k_{4''\rightarrow4'}$) between 0.09 and 0.58 s^{-1} and the population distribution of $p_{4'}/p_{4''}$ changing from 0.57/0.43 to 0.73/0.27, which agrees well with the values obtained from integration of peak volumes (0.50/0.50 to 0.65/0.35 in the corresponding temperature range).

Analysis of the temperature dependence of the equilibrium constant obtained from the microscopic exchange rates yielded a refolding enthalpy and entropy of $\Delta H_{4''\text{-}4'} = 11.2 \pm 1.1$ kcal mol^{-1} and $\Delta S_{4''\text{-}4'} = 38.1 \pm 3.7$ cal mol^{-1} K^{-1}. The temperature dependence of the equilibrium constant and the microscopic rate constants are shown in Figure 5. Thus, the results from the analysis of longitudinal exchange experiments are in line with those directly obtained from peak integration ($\Delta H_{4''\text{-}4'} = 9.9$ kcal mol^{-1}, $\Delta S_{4''\text{-}4'} = 33.1$ cal mol^{-1} K^{-1}). Assuming an *Arrhenius* temperature dependence of the rate constants, activation energies and approximated frequency factors $E^A_{4\#\text{-}4'} = 32.8 \pm 0.68$ kcal mol^{-1}/$A_{4\#\text{-}4'} = 10^{23.1}$ and $E^A_{4\#\text{-}4''} = 21.6 \pm 0.88$ kcal mol^{-1}/$A_{4\#\text{-}4''} = 10^{15.0}$ were obtained. The activation energy was found to amount to 55% (42%) of the (base pairing and stacking) enthalpy as computed by m-fold for fold **4′** (**4″**) (44). This makes a dissociative mechanism, which would imply a fully unfolded state, rather unlikely, but favors an associative mechanism with base pairs of both conformational states formed and being disrupted at the same time during the transition state (13).

Table 1. Microscopic rate constants and longitudinal relaxation rates along with errors obtained by longitudinal exchange experiments conducted on sequence **4** at each temperature analyzed

Temperature (K)	$k_{4'\rightarrow4''}$ (s^{-1})	$k_{4''\rightarrow4'}$ (s^{-1})	R_1(**4′**) (s^{-1})	R_1 (**4″**) (s^{-1})
298	0.051 ± 0.002	0.039 ± 0.002	2.13 ± 0.03	1.96 ± 0.04
300	0.065 ± 0.003	0.048 ± 0.003	2.26 ± 0.03	2.12 ± 0.03
303	0.102 ± 0.007	0.057 ± 0.004	2.46 ± 0.06	2.20 ± 0.06
306	0.191 ± 0.006	0.102 ± 0.005	2.59 ± 0.14	2.42 ± 0.16
310	0.419 ± 0.010	0.155 ± 0.004	2.30 ± 0.18	2.43 ± 0.23

Effective longitudinal relaxation rates are obtained by accounting for cross-correlated relaxation ('Materials and Methods' section and Supplementary Information).

The bistable RNA **4** was studied before in the temperature range between 283 and 298 K (12). The rate constants found at 298 K were compared to those determined previously at the same temperature and found to be in good agreement ($k_{4'\rightarrow4''} = 0.051\ s^{-1}$, $k_{4''\rightarrow4'} = 0.039\ s^{-1}$ in our work versus $k_{4'\rightarrow4''} = 0.091\ s^{-1}$, $k_{4''\rightarrow4'} = 0.076\ s^{-1}$ in

reference (12), see also Supplementary Table S4). The temperature dependence of the equilibrium constant is, however, more pronounced in our study, indicating larger enthalpy and entropy differences between the two conformers than previously reported (12). We find that fold **4″** (which contains the label within the base-paired region) is enthalpically destabilized with respect to **4′**. Over the observed temperature range, fold **4″** is, however, thermodynamically more stable than fold **4′**, indicating that fold **4″** is entropically favored over **4′**. The difference is reflected in the activation parameters of the backward reaction **4″** → **4′**, indicating that the enthalpic portion of the barrier (related to the activation energy) is smaller than for the forward reaction, whereas frequency factors indicate a larger entropic barrier. We believe that the discrepancy is due to the different temperature range and the lower pH employed in our study, as the effect of the uridine label is expected to only slightly stabilize secondary structures (see UV melting analysis in Supplementary Information).

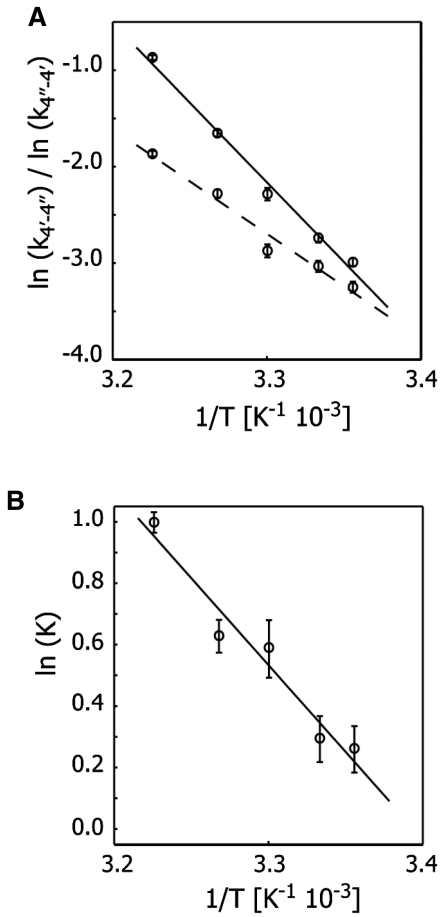

Figure 5. Analysis of the refolding reaction of sequence **4** in terms of kinetic and thermodynamic parameters obtained from longitudinal exchange experiments on the 2′-*O*-$^{13}CH_3$-uridine label. (**A**) ln ($k_{4'\rightarrow 4''}$) (solid line) and ln ($k_{4''\rightarrow 4'}$) (dashed line) as a function of the inverse temperature. (**B**) ln (K) [computed as ln ($k_{4'\rightarrow 4''}/k_{4''\rightarrow 4'}$)] as a function of 1/T. Error bars were obtained on the basis of duplicate data points by a Monte Carlo analysis, and regression was performed on averaged values of $k_{4'\rightarrow 4''}$, $k_{4''\rightarrow 4'}$, and K.

We subsequently applied the longitudinal exchange approach to the thermodynamically more stable 32 nt RNA stem loop structure **5** that coexists in two distinct conformations **5′** and **5″**. In order to ensure that the reaction was fast enough to be observable by this approach, experiments were conducted at elevated temperatures. For this RNA it was possible to obtain meaningful results from experiments conducted at 314 and 316 K. Respective correlation- and exchange-peak intensities as a function of mixing time are shown in Figure 6. The rate of interconversion at this temperature is in the same range as for sequence **4** at room temperature, i.e. $k_{5'\rightarrow 5''} = 0.348 \pm 0.063\,s^{-1}$ ($0.323 \pm 0.056\,s^{-1}$) and $k_{5''\rightarrow 5'} = 0.206 \pm 0.024\,s^{-1}$ ($0.262 \pm 0.024\,s^{-1}$) at 314 K (316 K). The complete set of kinetic parameters is given in Table 2. Due to the more pronounced skew in populations (approximately 7/3) as compared to RNA sequence **4**, the exchange peak derived from the less

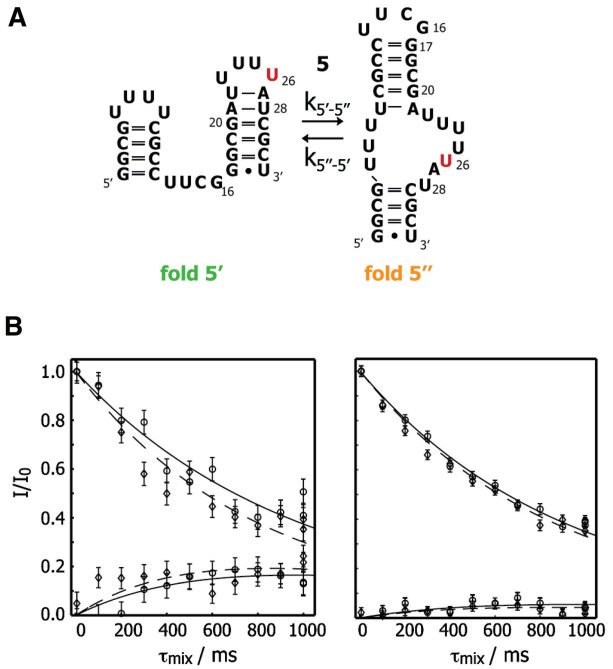

Figure 6. ^{13}C longitudinal exchange experiments conducted on sequence **5**. (**A**) Interconversion between conformations **5′** and **5″** with the uridine label highlighted in red. (**B**) Left panel: intensities of the corrrelation peak corresponding to conformation **5′** and exchange peak corresponding to transition **5′** → **5″** as a function of mixing time. Right panel: correlation peak pertinent to fold **5″** and exchange peak for the transition **5″** → **5′**. Results at 314 (316) K are depicted as circles (diamonds) and fits at 314 (316) K are shown as solid/dashed lines. Error bars were obtained on the basis of spectral noise in a Monte Carlo analysis.

Table 2. Microscopic rate constants and longitudinal relaxation rates along with errors obtained by longitudinal exchange experiments conducted on sequence **5** at each 314 and 316 K

Temperature (K)	$k_{5'\rightarrow 5''}$ (s^{-1})	$k_{5''\rightarrow 5'}$ (s^{-1})	R_1 (**5′**) (s^{-1})	R_1 (**5″**) (s^{-1})
314	0.348 ± 0.053	0.206 ± 0.024	0.67 ± 0.11	0.88 ± 0.05
316	0.323 ± 0.056	0.262 ± 0.024	0.92 ± 0.11	0.88 ± 0.05

populated species displays relatively low intensities in the longitudinal exchange experiments, which, in conjunction with a small rate of interconversion, impeded the acquisition of data of satisfactory signal-to-noise ratio below 314 K. On the other hand, rapid sample degradation and thermal denaturing effects did not permit extended exposure of this RNA to higher temperatures. The temperature range investigated for sequence **5** was thus too narrow to allow reliable determination of thermodynamic and kinetic information. For even more stable RNA structures and/or more skewed populations it is advisable to resort to real-time NMR techniques (14).

Application of longitudinal exchange experiments to the tristable RNA sequence **6** proved impractical due to spectral overlap of conformations **6″** and **6‴** in the proton dimension. In an attempt to obtain information about the kinetics of interconversion between the individual conformations we conducted ^{13}C CPMG relaxation dispersion measurements (21,27). CPMG relaxation dispersion experiments exploit the phenomenon that resonances show increased transverse relaxation rates if their chemical shifts are modulated by some conformational or chemical process. They permit the characterization of microsecond-to-millisecond motions and have become increasingly popular for detecting excited states, which are not sufficiently populated to be directly observable in NMR spectra. In the favorable case of exchange processes occurring in the intermediate regime on the chemical shift time-scale, the exchange rate constant k_{ex} (which is given by the sum of the forward and backward rate constants), the population of the individual states p_i, and the chemical shift difference between the states, $\Delta\omega$, can be obtained, as well as the relaxation rates at infinite CPMG field strength, $R_2^{\infty}(i,x)$, where i stands for the resonance and x stands for the spectrometer field strength. In the case of very slow or very fast exchange processes, not all exchange parameters can be obtained separately. If $k_{ex} >> \Delta\omega$ (fast exchange regime), k_{ex} can be accurately determined, along with the product of the populations and the square of the chemical shift differences, $p_a p_b \Delta\omega^2$ and $R_2^{\infty}(i,x)$. If exchange is slow on the chemical shift time-scale ($k_{ex} << \Delta\omega$) and the populations of both individual states are high enough to produce observable resonances, characteristic relaxation dispersion profiles are observed that can be analyzed as in Tollinger *et al.* (34). In this case, it is not possible to obtain the 'backward' rate constant (or the population of the excited state), such that only four parameters are obtained [the 'forward' rate constant k_{ab}, $\Delta\omega_{ab}$, and the two relaxation rates $R_2^{\infty}(i,x)$].

We recorded experiments at 300 K at 125 and 200 MHz carbon frequency. Small but statistically significant dispersion profiles could be found for conformers **6′** and **6‴** (the least populated conformer **6″** could not be analyzed due to low signal to noise ratio, Figure 7). In order to assess whether the underlying process is the slow exchange between the visible conformers, we analyzed the data using equations for two-state processes on the very slow, the intermediate and the fast time regimes (34,35). Also slow exchange in 2 three-state exchange models was investigated (Supplementary Table S5).

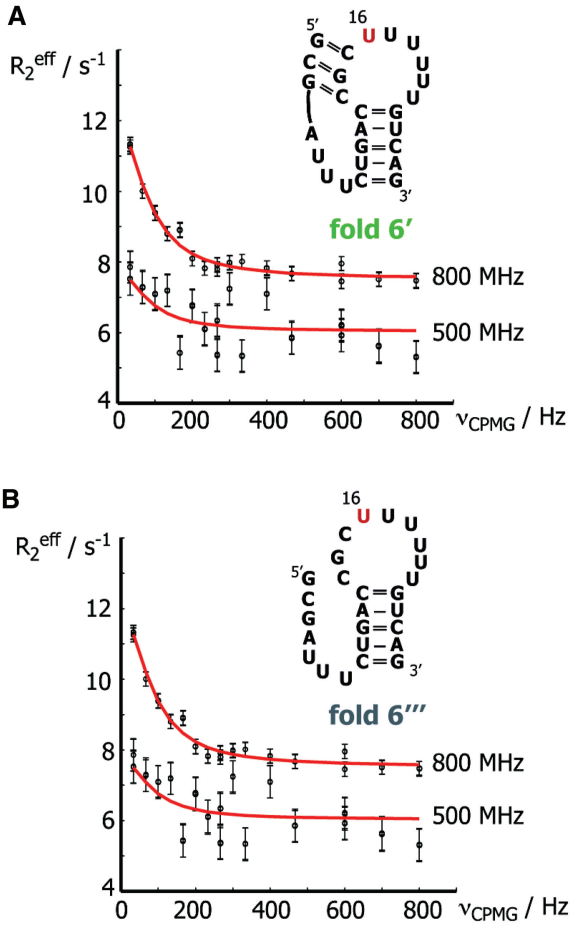

Figure 7. Analysis of CPMG relaxation dispersion of RNA sequence **6.** A two-state process that is fast on the chemical shift time-scale was fit to the data of conformer **6′** (**A**) and **6‴** (**B**) (for details of the fitting procedure see text and Supplementary Information). Experimental data points are shown as black circles and the fit is depicted as a red line. Spectrometer field strengths are indicated and the secondary structures of the two states are shown as inserts. Both conformers **6′** and **6‴** exchange with their respective excited state at a rate constant of ~500 s^{-1}.

From the magnetic field dependence of the exchange contribution to transverse relaxation in conjunction with the goodness of the fit of other models we concluded that in fact fast two-state exchange was suited to explain our experimental data (45). According to this model, conformers **6′** (**6‴**) access their excited states at rate constants of 593 ± 133 (460 ± 268) s^{-1}. From the fitted product function $p_a p_b \Delta\omega^2$ it follows that, depending on the relative populations, the chemical shift difference between the exchanging states are around 0.45 ppm (at an excited state population of 1%) and 0.8 ppm (at equimolar populations) for both conformers. The exact results are given in Table 3.

These results are surprising given the fact that we have obtained exchange peaks in a ^{13}C-^{13}C resolved 3D ZZ exchange experiment similar to the experiment conducted by Sprangers *et al.* (17) at mixing times of 5, 100 and 150 ms, indicating that species **6′** and **6‴** interchange on the order of 3 s^{-1} (Supplementary Figure S6). A process

Table 3. Results from CPMG relaxation dispersion experiments performed on sequence **6** at 300 K: two-state models

Two-state models	$k_{ex,6*-6**}$ (s^{-1})	k_{6*-6**} (s^{-1})	$P**$	$\Delta\omega$ (ppm)	$P*P** \Delta\omega^2$ (s^{-2}) (125 MHz)	χ^2_{red}
Conformer **6′**						
Slow (1)		2.92 ± 0.27		0.54 ± 0.05		0.61
Slow (2)		2.53 ± 0.13		1.10 ± 0.08		1.21
Intermediate	593 ± 133		0.20 ± 0.34	0.13 ± 0.09		3.13[a]
Fast	579 ± 62				1098 ± 90	0.34
Conformer **6‴**						
Slow (1)		3.79 ± 0.95		0.46 ± 0.12		0.30
Slow (2)		2.70 ± 0.50		1.07 ± 0.04		0.42
Intermediate	445 ± 300		0.58 ± 0.32	0.14 ± 0.10		1.82[a]
Fast	460 ± 268				1182 ± 461	0.27

Results are derived from 1000 Monte Carlo runs. The two states are tagged by asterisks, where one asterisk refers to the conformer which corresponds to the visible ground state (**6′** or **6‴**), and two asterisks represent the invisible excited state that pertains to it. For both analyzed resonances, the equation for slow exchange gave two solutions (1) and (2).
[a]χ^2_{red} values that are larger in the Monte Carlo analysis in comparison to the direct analysis. These discrepancies originate from the fact that the set of mean values derived from the Monte Carlo analysis does not represent the dispersion curve.

on this time-scale with the given populations and chemical shift differences would indeed lead to a dispersion profile of the observed size, albeit, with a different shape. From this discrepancy we conclude that we are in fact confronted with a mixture of several processes, i.e. the slow interconversion between conformers **6′** and **6‴** and their respective excursions to invisible conformers on the time scale of several hundred per second. For the parameters in our system it can be shown by numerical simulation that the dispersion profile obtained for a mixture of processes coincides within error with the one that would be obtained by a purely fast process (Supplementary Figure S7). Thus, it was not possible by the means of our data to separate the slow process, i.e. the interconversion between **6′** and **6‴**, from the dominant fast process. On the other hand, we may safely assume that the resulting parameters of the fast process have not been significantly perturbed by the presence of the slower one.

Given the positioning of the label it is tempting to infer that the observed excursion to an excited state might arise from the interconversion between different sugar puckers. However, such sugar pucker dynamics were recently determined to occur with exchange rates between 20 000 and 40 000 s^{-1}, i.e. about 40 times faster than the process we observe (21). Given this significant discrepancy, we tend to believe that the process we observe is not due to this fast conformational fluctuation but rather results from a local conformational dynamics in the 9 nt loop region (this structural feature is intact in both analyzed conformations). Further experiments using different label positions and/or types of labels are planned in order to investigate the nature of this dynamic event.

CONCLUSIONS

We used a 2′-*O*-$^{13}CH_3$-uridine label to study RNA refolding kinetics in an unperturbed equilibrium state, thereby circumventing a major disadvantage of methods that rely on the observation of exchange labile protons and enabling the study of RNA refolding phenomena at elevated temperatures (15).

First, we used the label to assign and quantify fold populations of multi-stable RNAs. The ^{13}C-modification proved to be minimally invasive, as no population changes and only minor melting point changes were observed compared to the wild-type sequences (8). The refolding kinetics of RNA **4** could be determined using a ^{13}C longitudinal exchange experiment at temperatures ranging from 298 to 310 K. The obtained rate constants were in good agreement with previous findings (12). The subsequent *Arrhenius* analysis yielded an estimation of the transition state energy between the two competing secondary structures.

We extended the approach to the more stable RNA sequence **5** comprising 32 nt. As expected, exchange peaks were found only at elevated temperature (>313 K). It was possible to determine the folding kinetics at 314 and 316 K. Not only the velocity of the process but also the skew in populations poses a limitation to the sensitivity of this approach. For more stable structures or bistable RNAs with very skewed populations, it is advisable to address the refolding kinetics by real-time NMR methods as previously shown (11).

For the tristable RNA **6** longitudinal exchange experiments were impractical due to poor chemical shift dispersion in the proton dimension. As an alternative approach we used ^{13}C CPMG relaxation dispersion NMR spectroscopy. Relaxation dispersion data pointed to a process that is fast on the chemical shift time-scale with $k_{ex} \sim 500\ s^{-1}$ and $\Delta\omega \geq 0.3$ ppm for at least two of the species. A slow process, detected by ^{13}C-^{13}C resolved ZZ-exchange experiments, is obscured by the dispersion profile of the fast process.

Our 2′-*O*-$^{13}CH_3$-uridine label has proven to be generally applicable to study conformational heterogeneity and the refolding kinetics in small to mid-sized RNAs comprising up to ~35 nt using standard NMR techniques. For even larger molecules, the signal-to-noise limitation could be alleviated by using cryogenic probes along with TROSY variants of the NMR experiments (17,46). The labeling procedure itself is feasible for RNAs of up to 150 nt using the recently developed approach that combines

chemical RNA synthesis and enzymatic ligation methods (47,48).

Compared to other non-native NMR labeling approaches for RNA, like incorporation of 5-F-uridine, we think that our presented approach is as minimally invasive as the fluorine tag (49–52). Furthermore, we consider the 2′-*O*-$^{13}CH_3$ labeling protocol more versatile as triple resonance probes to carry out the ^{13}C-based experiments are more disseminated in the biomolecular NMR community than probes suitable for the ^{19}F-based experiments.

In principle, similar 2′-*O*-$^{13}CH_3$ labeling schemes can be applied to all 4 nt types conveying a high level of versatility to the labeling approach. It will also be very interesting to introduce the ^{13}C-methoxy-residue into RNAs where this very modification occurs naturally. Subsequent NMR spectroscopic analysis can be used to gain interesting insight into the structure and function of the methoxy-modification.

SUPPLEMENTARY DATA

Supplementary Data are available at NAR Online.

ACKNOWLEDGEMENTS

C.K. thanks Ronald Micura (Innsbruck) and Bernhard Kräutler (Innsbruck) for continuous support and scientific discussions. K.K. was a recipient of an APART fellowship of the Austrian Academy of Sciences at the time when this study was realized.

FUNDING

FWF (V173 to K.K., SFB-17 and P20549 to R.K.). Funding for open access charge: FWF - Austrian Science Fund.

Conflict of interest statement. None declared.

REFERENCES

1. Coppins,R.L., Hall,K.B. and Groisman,E.A. (2007) The intricate world of riboswitches. *Curr. Opin. Microbiol.*, **10**, 176–181.
2. Dambach,M.D. and Winkler,W.C. (2009) Expanding roles for metabolite-sensing regulatory RNAs. *Curr. Opin. Microbiol.*, **12**, 161–169.
3. Schwalbe,H., Buck,J., Fürtig,B., Noeske,J. and Wöhnert,J. (2007) Structures of RNA Switches: insight into Molecular Recognition and Tertiary Structure. *Angew Chem. Int. Ed. Engl.*, **46**, 1212–1219.
4. Serganov,A. (2009) The long and the short of riboswitches. *Curr. Opin. Struct. Biol.*, **19**, 251–259.
5. Tucker,B.J. and Breaker,R.R. (2005) Riboswitches as versatile gene control elements. *Curr. Opin. Struct. Biol.*, **15**, 342–348.
6. Narberhaus,F., Waldminghaus,T. and Chowdhury,S. (2006) RNA thermometers. *FEMS Microbiol. Rev.*, **30**, 3–16.
7. Flamm,C., Hofacker,I.L., Maurer-Stroh,S., Stadler,P.F. and Zehl,M. (2001) Design of multistable RNA molecules. *RNA*, **7**, 254–265.
8. Höbartner,C. and Micura,R. (2003) Bistable secondary structures of small RNAs and their structural probing by comparative imino proton NMR spectroscopy. *J. Mol. Biol.*, **325**, 421–431.
9. Micura,R. and Höbartner,C. (2003) On secondary structure rearrangements and equilibria of small RNAs. *ChemBioChem*, **4**, 984–990.
10. Schultes,E.A. and Bartel,D.P. (2000) One sequence, two ribozymes: implications for the emergence of new ribozyme folds. *Science*, **289**, 448–452.
11. Fürtig,B., Wenter,P., Reymond,L., Richter,C., Pitsch,S. and Schwalbe,H. (2007) conformational dynamics of bistable RNAs studied by time-resolved NMR spectroscopy. *J. Am. Chem. Soc.*, **129**, 16222–16229.
12. Wenter,P., Fürtig,B., Hainard,A., Schwalbe,H. and Pitsch,S. (2006) A caged uridine for the selective preparation of an RNA fold and determination of its refolding kinetics by real-time NMR. *ChemBioChem*, **7**, 417–420.
13. Wenter,P., Fürtig,B., Hainard,A., Schwalbe,H. and Pitsch,S. (2005) Kinetics of photoinduced RNA refolding by real-time NMR spectroscopy. *Angew Chem. Int. Ed. Engl.*, **44**, 2600–2603.
14. Fürtig,B., Buck,J., Manoharan,V., Bermel,W., Jäschke,A., Wenter,P., Pitsch,S. and Schwalbe,H. (2007) Time-resolved NMR studies of RNA folding. *Biopolymers*, **86**, 360–383.
15. Wenter,P., Bodenhausen,G., Dittmer,J. and Pitsch,S. (2006) Kinetics of RNA refolding in dynamic equilibrium by 1H-detected 15 N exchange NMR spectroscopy. *J. Am. Chem. Soc.*, **128**, 7579–7587.
16. Farrow,N.A., Zhang,O., Forman-Kay,J.D. and Kay,L.E. (1995) Comparison of the backbone dynamics of a folded and an unfolded SH3 domain existing in equilibrium in aqueous buffer. *Biochemistry*, **34**, 868–878.
17. Sprangers,R., Gribun,A., Hwang,P.M., Houry,W.A. and Kay,L.E. (2005) Quantitative NMR spectroscopy of supramolecular complexes: dynamic side pores in ClpP are important for product release. *Proc. Natl Acad. Sci. USA*, **102**, 16678–16683.
18. Puglisi,J.D., Wyatt,J.R. and Tinoco,J.I. (1990) Conformation of an RNA pseudoknot. *J. Mol. Biol.*, **214**, 437–453.
19. Puglisi,J.D., Wyatt,J.R. and Thomas,L.J. (1995) *Methods in Enzymology*, Vol. 261. Academic Press, United States, pp. 323–350.
20. Palmer,A.G. 3rd, Kroenke,C.D. and Loria,J.P. (2001) Nuclear magnetic resonance methods for quantifying microsecond-to-millisecond motions in biological macromolecules. *Methods Enzymol.*, **339**, 204–238.
21. Johnson,J.E. and Hoogstraten,C.G. (2008) Extensive backbone dynamics in the GCAA RNA tetraloop analyzed using 13C NMR spin relaxation and specific isotope labeling. *J. Am. Chem. Soc.*, **130**, 16757–16769.
22. Yamazaki,T., Muhandiram,R. and Kay,L.E. (1994) NMR experiments for the measurement of carbon relaxation properties in highly enriched, uniformly 13C,15N-labeled proteins: application to 13C.alpha. carbons. *J. Am. Chem. Soc.*, **116**, 8266–8278.
23. Vallurupalli,P., Scott,L., Williamson,J. and Kay,L. (2007) Strong coupling effects during X -pulse CPMG experiments recorded on heteronuclear ABX spin systems: artifacts and a simple solution. *J. Biomol. NMR*, **38**, 41–46.
24. Lundström,P., Hansen,D. and Kay,L. (2008) Measurement of carbonyl chemical shifts of excited protein states by relaxation dispersion NMR spectroscopy: comparison between uniformly and selectively 13C labeled samples. *J. Biomol. NMR*, **42**, 35–47.
25. Johnson,J.E., Julien,K.R. and Hoogstraten,C.G. (2006) Alternate-site isotopic labeling of ribonucleotides for NMR studies of ribose conformational dynamics in RNA. *J. Biomol. NMR*, **35**, 261–274.
26. Hansen,A.L., Nikolova,E.N., Casiano-Negroni,A. and Al-Hashimi,H.M. (2009) Extending the range of microsecond-to-millisecond chemical exchange detected in labeled and unlabeled nucleic acids by selective carbon R1œÅ NMR spectroscopy. *J. Am. Chem. Soc.*, **131**, 3818–3819.
27. Skrynnikov,N.R., Mulder,F.A., Hon,B., Dahlquist,F.W. and Kay,L.E. (2001) Probing slow time scale dynamics at methyl-containing side chains in proteins by relaxation dispersion NMR measurements: application to methionine residues in a cavity mutant of T4 lysozyme. *J. Am. Chem. Soc.*, **123**, 4556–4566.

28. Kreutz,C., Kahlig,H., Konrat,R. and Micura,R. (2005) Ribose 2′-F labeling: a simple tool for the characterization of RNA secondary structure equilibria by 19F NMR spectroscopy. *J. Am. Chem. Soc.*, **127**, 11558–11559.
29. Hwang,T.L. and Shaka,A.J. (1995) water suppression that works. excitation sculpting using arbitrary wave-forms and pulsed-field gradients. *J. Magn. Reson. Series A*, **112**, 275–279.
30. Wenter,P. and Pitsch,S. (2003) Synthesis of selectively 15N-labeled 2′-O-{[(triisopropylsilyl)oxy]methyl}(=tom)-protected ribonucleoside phosphoramidites and their incorporation into a bistable 32mer RNA sequence. *Helvetica Chimica Acta*, **86**, 3955–3974.
31. Plateau,P. and Gueron,M. (1982) Exchangeable proton NMR without base-line distorsion, using new strong-pulse sequences. *J. Am. Chem. Soc.*, **104**, 7310–7311.
32. Delaglio,F., Grzesiek,S., Vuister,G.W., Zhu,G., Pfeifer,J. and Bax,A. (1995) NMRPipe: a multidimensional spectral processing system based on UNIX pipes. *J. Biomol. NMR*, **6**, 277–293.
33. Rischel,C. (1995) Fundamentals of peak integration. *J. Magn. Reson. Series A*, **116**, 255–258.
34. Tollinger,M., Skrynnikov,N.R., Mulder,F.A., Forman-Kay,J.D. and Kay,L.E. (2001) Slow dynamics in folded and unfolded states of an SH3 domain. *J. Am. Chem. Soc.*, **123**, 11341–11352.
35. Luz,Z. and Meiboom,S. (1963) Nuclear magnetic resonance study of the protolysis of trimethylammonium ion in aqueous solution—order of the reaction with respect to solvent. *J. Chem. Phys.*, **39**, 366–370.
36. Lesnik,E.A. and Freier,S.M. (1998) What affects the effect of 2′-O-alkoxy modifications? 1. stabilization effect of 2′-O-methoxy substitutions in uniformly modified DNA oligonucleotides. *Biochemistry*, **37**, 6991–6997.
37. Fohrer,J., Hennig,M. and Carlomagno,T. (2006) Influence of the 2′-hydroxyl group conformation on the stability of A-form helices in RNA. *J. Mol. Biol.*, **356**, 280–287.
38. Hennig,M., Fohrer,J. and Carlomagno,T. (2005) Assignment and NOE analysis of 2′-hydroxyl protons in RNA: implications for stabilization of RNA A-form duplexes. *J. Am. Chem. Soc.*, **127**, 2028–2029.
39. Giedroc,D.P., Cornish,P.V. and Hennig,M. (2003) Detection of scalar couplings involving 2′-hydroxyl protons across hydrogen bonds in a frameshifting mrna pseudoknot. *J. Am. Chem. Soc.*, **125**, 4676–4677.
40. Höbartner,C. and Micura,R. (2004) Chemical synthesis of selenium-modified oligoribonucleotides and their enzymatic ligation leading to an U6 SnRNA stem-loop segment. *J. Am. Chem. Soc.*, **126**, 1141–1149.
41. McGee,D.P.C. and Zhai,Y. (1996) Reaction of anhydronucleosides with magnesium alkoxides: regiospecific synthesis of 2′-O-alkylpyrimidine nucleosides. *Nucleosides Nucleotides Nucleic Acids*, **15**, 1797–1803.
42. Al-Hashimi,H.M. and Walter,N.G. (2008) RNA dynamics: it is about time. *Curr. Opin. Struct. Biol.*, **18**, 321–329.
43. Tollinger,M., Neale,C., Kay,L.E. and Forman-Kay,J.D. (2006) Characterization of the hydrodynamic properties of the folding transition state of an SH3 domain by magnetization transfer NMR spectroscopy. *Biochemistry*, **45**, 6434–6445.
44. Zuker,M. (2003) Mfold web server for nucleic acid folding and hybridization prediction. *Nucleic Acids Res.*, **31**, 3406–3415.
45. Millet,O., Loria,J.P., Kroenke,C.D., Pons,M. and Palmer,A.G. (2000) The static magnetic field dependence of chemical exchange linebroadening defines the nmr chemical shift time scale. *J. Am. Chem. Soc.*, **122**, 2867–2877.
46. Religa,T.L., Sprangers,R. and Kay,L.E. (2010) Dynamic regulation of archaeal proteasome gate opening as studied by TROSY NMR. *Science*, **328**, 98–102.
47. Lang,K. and Micura,R. (2008) The preparation of site-specifically modified riboswitch domains as an example for enzymatic ligation of chemically synthesized RNA fragments. *Nat. Protocols*, **3**, 1457–1466.
48. Rieder,R., Hobartner,C. and Micura,R. (2009) Enzymatic ligation strategies for the preparation of purine riboswitches with. *Methods Mol. Biol.*, **540**, 15–24.
49. Puffer,B., Kreutz,C., Rieder,U., Ebert,M.-O., Konrat,R. and Micura,R. (2009) 5-Fluoro pyrimidines: labels to probe DNA and RNA secondary structures by 1D 19F NMR spectroscopy. *Nucleic Acids Res.*, **37**, 7728–7740.
50. Rieder,U., Kreutz,C. and Micura,R. (2010) Folding of a transcriptionally acting PreQ1 riboswitch. *Proc. Natl Acad. Sci.*, **107**, 10804–10809.
51. Hennig,M., Scott,L.G., Sperling,E., Bermel,W. and Williamson,J.R. (2007) Synthesis of 5-fluoropyrimidine nucleotides as sensitive NMR probes of RNA structure. *J. Am. Chem. Soc.*, **129**, 14911–14921.
52. Scott,L.G., Geierstanger,B.H., Williamson,J.R. and Hennig,M. (2004) Enzymatic synthesis and 19F NMR studies of 2-fluoroadenine-substituted RNA. *J. Am. Chem. Soc.*, **126**, 11776–11777.